SCIENCE CHINA
Chemistry

•ARTICLES•

September 2022 Vol.65 No.9: 1782–1790
https://doi.org/10.1007/s11426-022-1317-0

Polydiacetylene-based poly-ion complex enabling aggregation-induced emission and photodynamic therapy dual turn-on for on-demand pathogenic bacteria elimination

Sidan Tian[1†], Yuan Lu[1†], Zhenyan He[1], Qiang Yue[1], Zhiyong Zhuang[1], Yingzhou Wang[4], Fanling Meng[1] & Liang Luo[1,2,3*]

[1]*National Engineering Research Center for Nanomedicine, College of Life Science and Technology, Huazhong University of Science and Technology, Wuhan 430074, China;*
[2]*Key Laboratory of Molecular Biophysics of the Ministry of Education, College of Life Science and Technology, Huazhong University of Science and Technology, Wuhan 430074, China;*
[3]*Hubei Key Laboratory of Bioinorganic Chemistry and Materia Medica, School of Chemistry and Chemical Engineering, Huazhong University of Science and Technology, Wuhan 430074, China;*
[4]*College of Life Science and Technology, Wuhan Polytechnic University, Wuhan 430023, China*

Received April 23, 2022; accepted June 23, 2022; published online August 16, 2022

Poly-ion complex (PIC) integrating non-antibiotic theranostics holds great promise in the combat against drug-resistant bacteria. Photosensitizers with aggregation-induced emission (AIE) characteristic are particularly intriguing theranostic agents, but incorporating them into antibacterial PIC to enable both fluorescence and reactive oxygen species (ROS) generation turn-on is deemed a great challenge. Here we report the development of a PIC that can dually boost the fluorescence and ROS generation in the presence of pathogen bacteria. The PIC is constructed based on an anionic polydiacetylene poly(deca-4,6-diynedioic acid) (PDDA), which completely degrades in the presence of ROS. A cationic polymer quaternized poly(2-(dimethylamino)ethyl methacrylate) (PQDMA) that can disrupt bacterial membrane is co-loaded together with a highly efficient AIE photosensitizer TPCI in the PIC. PIC is nonfluorescent initially in that PDDA can quench the AIE of TPCI in PIC. When pathogenic bacteria are present, they can disturb the assembly of PIC to release TPCI, whose fluorescence turns on sensitively to indicate the existence of bacteria. The on-demand irradiation can be subsequently applied to excite TPCI, which generates ROS to degrade PDDA and deform the PIC. As a result, TPCI and PQDMA are completely released to eliminate bacteria through a synergy of turned-on photodynamic therapy (PDT) and membrane disruption. The highly efficient detection and inhibition against both Gram-negative and Gram-positive bacteria have validated this polydiacetylene-based PIC system as an effective non-antibiotic antibacterial theranostic platform as well as a new strategy to enable "turn-on" fluorescence sensing and imaging of AIE fluorophores.

poly-ion complex, ROS responsive, polydiacetylene, photodynamic therapy, aggregation-induced emission

Citation: Tian S, Lu Y, He Z, Yue Q, Zhuang Z, Wang Y, Meng F, Luo L. Polydiacetylene-based poly-ion complex enabling aggregation-induced emission and photodynamic therapy dual turn-on for on-demand pathogenic bacteria elimination. *Sci China Chem*, 2022, 65: 1782–1790, https://doi.org/10.1007/s11426-022-1317-0

†These authors contributed equally to this work.
*Corresponding author (email: liangluo@hust.edu.cn)

1 Introduction

Pathogenic bacterial infection has been a mortal threat for human health for centuries. Since the first discovery of penicillin in 1928, antibiotics have revolutionized the human's battle to fight against bacterial infection [1–3]. However, bacteria are becoming more and more resistant to antibiotics, given the widespread abuse of antibiotics in recent decades [4–7]. Non-antibiotic inhibition of pathogenic bacteria is in urgent clinical need to effectively control various infections [8–10]. To date, tremendous efforts have been made to explore new strategies and to fabricate new materials for non-antibiotic pathogen inhibition, including metal ions [11], chitosan [12,13], antibacterial peptides [14,15], and synthetic cationic polymers [16,17]. Well-established clinical therapies such as photodynamic therapy (PDT) and photothermal therapy (PTT) are also considered as potential alternatives against antibiotic-resistant bacteria [18–21]. Unlike the antibiotics that kill pathogens through biological processes, the non-antibiotic antibacterial approaches based on chemical or physical damages are more powerful to suppress the pathogenic bacteria with little resistance [22,23]. However, non-antibiotic strategies suffer from severe side effects in that they are usually non-selective and unable to distinguish microorganisms from human cells.

Nanocarrier-based drug delivery system represents a promising solution to enable the target-preferential delivery of therapeutic agents with controlled release kinetics at the infection lesions [24,25]. Nanocarriers can also co-deliver multiple therapeutic and imaging agents for integrated combinational therapy and concurrent diagnosis [26–29]. Furthermore, by elegantly designing nanocarriers, one could achieve desired release of the agents in infection-related microenvironments [30–32] or external stimulations such as photo irradiation, ultrasonic, or magnetic fields [33–38]. More interestingly, nanocarrier-based "on-demand" therapy with precise spatiotemporal control can maximize the efficacy of the antibacterial agents with minimal side effects [39]. Photosensitizers with aggregation-induced emission (AIE) characteristics are ideal candidates to enable the "on-demand" therapy, attributed to their intrinsic fluorescence reporting and reactive oxygen species (ROS) generating features. Different from those fluorophores whose fluorescence may quench at high concentrations or in aggregated state, AIE photosensitizers are non-emissive when molecularly dissolved, but can "turn-on" their fluorescence emission upon aggregation or restriction of intramolecular motion [40–42]. However, AIE photosensitizers are usually in aggregated state when loaded in nanocarriers, so that their fluorescence is in an already "turned on" state [43]. When released from the nanocarriers, these AIE fluorophores have to work in a "turn-off" or "always-on" manner. It is therefore highly desired to develop a smart nanocarrier system to warrant the fluorescence "turn-on" of AIE photosensitizers to assure the "on-demand" therapy.

In this work, we have created a ROS-deformable poly-ion complex (PIC) to approach AIE "turn-on" detection and on-demand eradication of pathogenic bacteria. Through electrostatic interaction, the PIC is composed of an anionic polydiacetylene poly(deca-4,6-diynedioic acid) (PDDA), which completely degrades in the presence of ROS [44], a cationic polymer quaternized poly(2-(dimethylamino)ethyl methacrylate) (PQDMA) that can disrupt bacterial membrane [45,46], and a highly efficient cationic AIE photosensitizer TPCI. The ultraviolet-visible (UV-vis) absorption spectrum of PDDA is partially overlapped with the fluorescence spectrum of TPCI, so that it can quench the fluorescence of TPCI in the PIC due to the fluorescence resonance energy transfer effect. When bacteria are present, their strong negatively-charged surfaces can provide a competitive interaction with the cationic TPCI and PQDMA, so as to selectively disturb the assembly of PIC and release partial TPCI. The separated TPCI can easily capture the bacteria, and turn on its AIE fluorescence through intramolecular motion restriction to show the existence of bacteria. Moreover, once we observe the bacterial infection by the TPCI fluorescence, the on-demand irradiation can be triggered to excite TPCI. The generated ROS therefore degrade PDDA and consequently deform the PIC to burst release all of the TPCI and PQDMA, which eliminate bacteria through synergistic membrane disruption and enhanced PDT. The detection and inhibition activities of the PIC against both Gram-negative (*E. coli*) and Gram-positive (*S. aureus*) bacteria have been proved to be very efficient at low concentrations, and we also validated the antibacterial efficacy of PIC in *P. aeruginosa*-infected mouse model. This ROS-deformable PIC system not only demonstrates great potential in combating bacterial infection, but also paves a new way to enable "turn-on" fluorescence sensing and imaging of AIE fluorophores (Figure 1).

2 Results and discussion

2.1 Preparation and characterization of PIC

We firstly synthesized PDDA using host-guest topochemical polymerization and isolated it following a previously reported procedure [47]. PDDA was further functionalized with polyethylene glycol (PEG, 25% molar ratio of the carboxyl groups on PDDA) following typical esterification conditions to increase the stability of the PIC [47]. The reaction mixture was dialyzed against water to obtain the purified PEG-PDDA. The cationic antibacterial agents TPCI and PQDMA were then employed to form the PIC with PEG-PDDA (Figure 2a). TPCI is ultraefficient in generating ROS

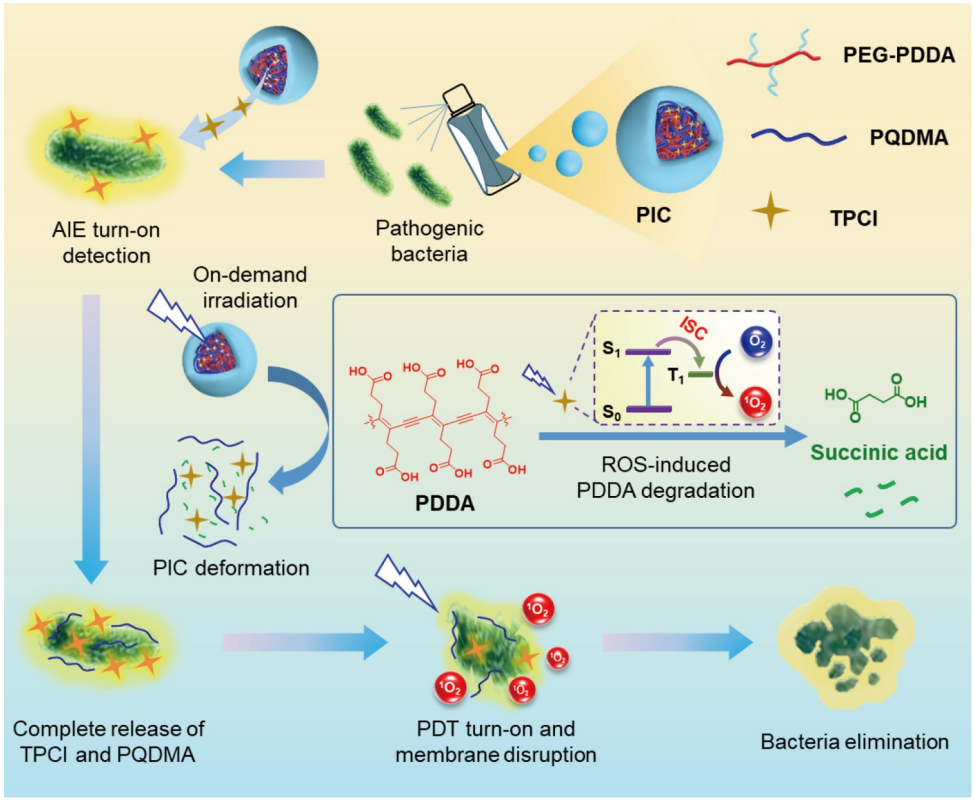

Figure 1 Schematic illustration of the bacterial AIE turn-on detection and synergistic antibacterial process by the ROS-deformable PIC (color online).

upon white light irradiation, with a >90% ROS quantum yield [48]. In addition, TPCI is an AIE photosensitizer carrying four terminal pyridinium groups (Figure 2a), which can facilitate the binding with anionic bacteria. PQDMA is a poly quaternary ammonium salt with high density positive charges, which can induce the irreversible structural damage to bacterial cell membranes through their strong electrostatic interactions.

The formation of PIC could be guided by the positive-to-negative (p/n) charge ratio. When the ratio reached 1, the resulting mixture was dialysed to remove free molecules. The transmission electronic microscopy (TEM) images revealed that the prepared PIC nanoparticles showed uniform sizes of 50 to 100 nm (Figure 2b). The particle size of the PIC was also confirmed by dynamic laser light scattering (DLS, Figure 2c). The samples with different p/n ratios were tested with DLS to trace the formation of the PIC (Figure S1, Supporting Information online). When the p/n ratio reached 0.8, the PIC showed minimal particle size and the strongest scattered intensity. Next, we tested the zeta potential of the PIC in comparison with individual component (Figure 2d). The zeta potential values of PEG-PDDA, TPCI, and PQDMA were −30, +50, and +20 mV, respectively. As expected, the formed PIC showed a zeta potential close to zero, suggesting it is neutrally charged. To illustrate the quenching effect of PDDA to the AIE of aggregated TPCI in PIC, we employed an anionic polymer without fluorescence quenching effect (polyacrylic acid, PAA) as a control to form the PIC with TPCI and PQDMA. As expected, the fluorescence of TPCI significantly increased with the addition of PAA (Figure 2e) or bovine serum albumin (BSA), a typical negatively charged protein (Figure S2). In a sharp contrast, when the anionic PDDA was added to the TPCI solution, no detectable fluorescence was observed (Figure 2f). The remarkable difference in the normalized TPCI fluorescence between adding PAA and PDDA unambiguously indicated the strong quenching effect of PDDA (Figure 2g).

2.2 Fluorescence “turn-on” detection of bacteria with PDDA-based PIC

The successful quenching of TPCI fluorescence in PIC inspired us to pursue the fluorescence “turn-on” detection of bacteria. The strong negatively charged surface of bacteria could competitively interact with the cationic TPCI and PQDMA in the PIC, leading to the partial disintegration of PIC and the release of small molecule TPCI. The separated TPCI was then able to “turn-on” its fluorescence when it attached to the bacteria surface (Figure 3a). Using *E. coli* as a model pathogen, we examined the capability of our PIC in detecting bacteria *in vitro*. As shown in Figure 3b, c, the fluorescence intensity of TPCI gradually increased with the

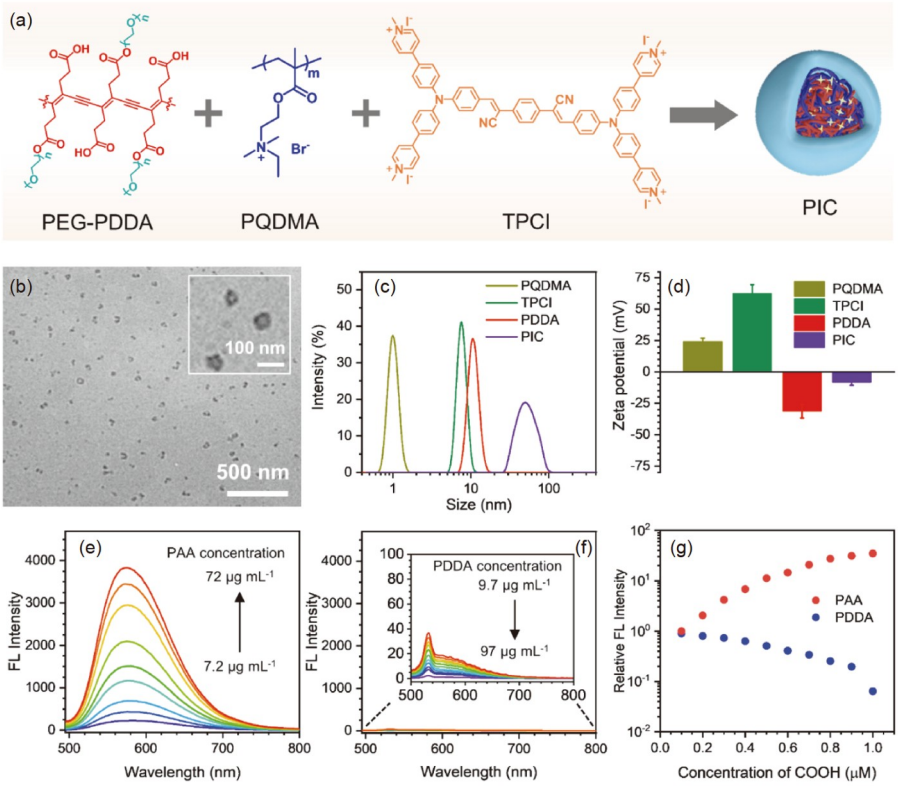

Figure 2 Preparation and characterization of PIC. (a) Schematic illustration of the formation of PIC by PEG-PDDA, PQDMA, and TPCI. (b) TEM image of formed PIC. (c) Size distributions of PEG-PDDA, PQDMA, TPCI, and PIC measured by DLS. (d) Zeta potentials of PEG-PDDA, PQDMA, TPCI, and PIC measured by DLS. Fluorescence (FL) spectrum of TPCI with the increase of PAA concentration (e) and PDDA concentration (f). (g) Relative fluorescence intensity of TPCI as a function of carboxyl group in PAA and PDDA (color online).

increase of the bacteria concentration. The turn-on procedure of the AIE fluorescence of the bacteria solution could also be observed using a fluorescence microscopy (Figure 3d). The free TPCI concentration is only 3.7 nM in solution after being absorbed by bacteria, which evidenced the strong binding affinity of TPCI with the bacteria (Figure S3a). With the increase of TPCI concentration, its fluorescence increased both in the absence (Figure S4) or presence of bacteria (Figure S5). We further determined that the "turn-on" detection of bacteria by PIC has a detection limit of 1×10^5 CFU mL^{-1} for Gram-negative bacteria (Figure S3b) and 0.5×10^5 CFU mL^{-1} for Gram-positive bacteria (Figure S3c). We also used confocal laser scanning microscopy (CLSM) to observe the bacteria at different concentrations after being treated with PIC (Figure 3e). The CLSM images evidenced the strong fluorescence of TPCI on the surface of the bacteria, and demonstrated that the detection limit of PIC on both *E. coli* and *S. aureus* could be as low as 1×10^3 CFU mL^{-1}. The above results clearly proved the successful AIE turn-on detection and imaging of both Gram-negative and Gram-positive bacteria with high sensitivity, taking the advantage of both high binding affinity of TPCI with bacterial surface and strong quenching effect of PDDA.

2.3 On-demand bacteria elimination by turned-on PDT and membrane disruption

The sensitive "turn-on" detection of the bacteria also enabled the on-demand antibacterial therapy by the ROS-deformable PIC. After the presence of bacteria was verified by the lightening of TPCI fluorescence, light irradiation could be applied on demand to activate PIC for bacteria elimination (Figure 4a). TPCI could efficiently generate large quantity of ROS upon 450 nm irradiation, and deform the PIC by degrading the skeleton PDDA to completely release TPCI and PQDMA. To verify the degradation of PDDA by TPCI-generated ROS, we applied 450 nm irradiation on a mixed solution of TPCI and PDDA. The absorbance (Figure 4b) and Raman intensity (Figure 4c) of PDDA diminished gradually with the increase of the irradiation time, indicating the steady degradation of PDDA in the presence of TPCI-generated ROS. The ^{1}H nuclear magnetic resonance (^{1}H NMR) of the final degradation product of PDDA was no longer the same as that of PDDA, but identical to a small molecule of succinic acid, consistent with the previously reported photooxidative degradation product of PDDA [44].

The ROS generation of PIC was determined by a probe 2′,7′-dichlorodihydrofluorescein diacetate (DCFDA) in

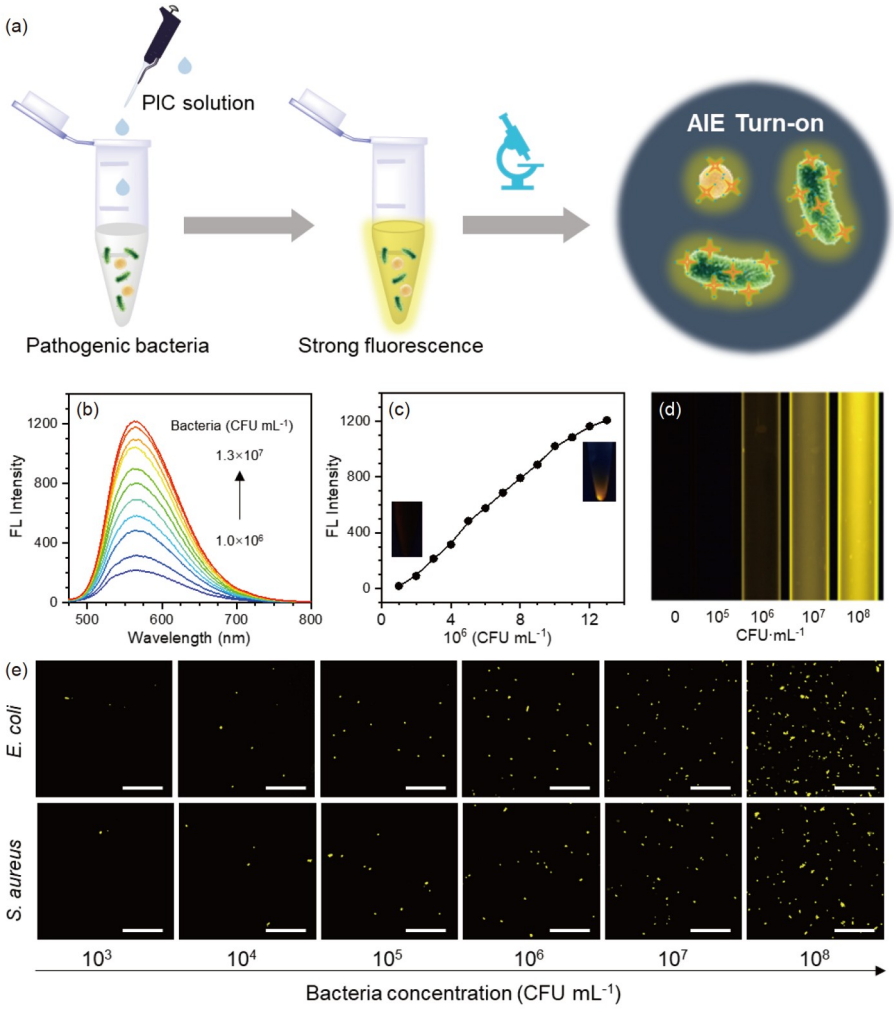

Figure 3 Fluorescence detection of bacteria with poly-ion complex nanoparticles. (a) Illustration of bacterial detection by AIE turn-on of TPCI in the PIC. (b) Fluorescence spectra of TPCI with increased bacteria concentration. (c) Quantification of the maximal fluorescence intensity with different bacteria concentrations. (d) Fluorescence images of PIC containing solutions with different numbers of bacteria. Solution in a glass capillary was excited with blue light (λ=450 nm) and imaged with a fluorescence microscope. (e) Confocal images of PIC treated bacteria with different concentrations (λ_{ex}=488 nm; λ_{em}= 600–650 nm). Scale bar: 50 μm (color online).

water (Figure 4e). Interestingly, when TPCI was loaded into the PDDA-based PIC, the ROS generation detected by the DCFDA probe remained low, suggesting that the quenching effect of PDDA not only reduced the fluorescence emission of TPCI but also restrained the ROS generation process. Strikingly, in the presence of *E. coli*, the ROS generation of PIC was significantly boosted, implying that the ROS generation of PIC was also turned on in the presence of bacteria. To evaluate the antibacterial activity of the PIC, *E. coli* was treated with different agents and then incubated in the culture media. The activity of the remaining bacteria was examined by measuring the change of optical density at 600 nm (OD_{600}) in typical incubation condition. Upon 450 nm light irradiation, which is non-toxic to bacteria (Figure S6), PIC exhibited a significantly enhanced inhibition on bacteria growth than the free TPCI (Figure 4f), or the sole PQDMA and PDDA (Figure 4g). The quantitative analysis of the half maximal inhibitory concentration (IC_{50}) of the antibacterial agents was compiled in Figure 4h, in which PIC showed the lowest inhibition concentration compared with individual antibacterial agents. On the other hand, the TPCI without light and the PDDA carrier showed no antibacterial activity. We also used the colony counting experiments to evaluate the antibacterial activity of the PIC (Figure 4i, Figures S7 and S8). The results evidenced that PDDA itself had no antibacterial activity, but the PDDA-based PIC had a superior antibacterial activity compared with PQDMA and irradiated TPCI. The scanning electronic microscopic (SEM) images revealed that PIC induced severe membrane disruption of the bacteria. Compared with the intact membrane structure of *E. coli* (Figure 4j), we observed crumpled bacterial surface and aggregation of the bacteria after PIC incubation, even without light irradiation (Figure 4k). The result suggested the PQDMA in PIC maintain its membrane binding and disruption property in the presence of bacteria. The antibacterial activity of PIC was also validated on

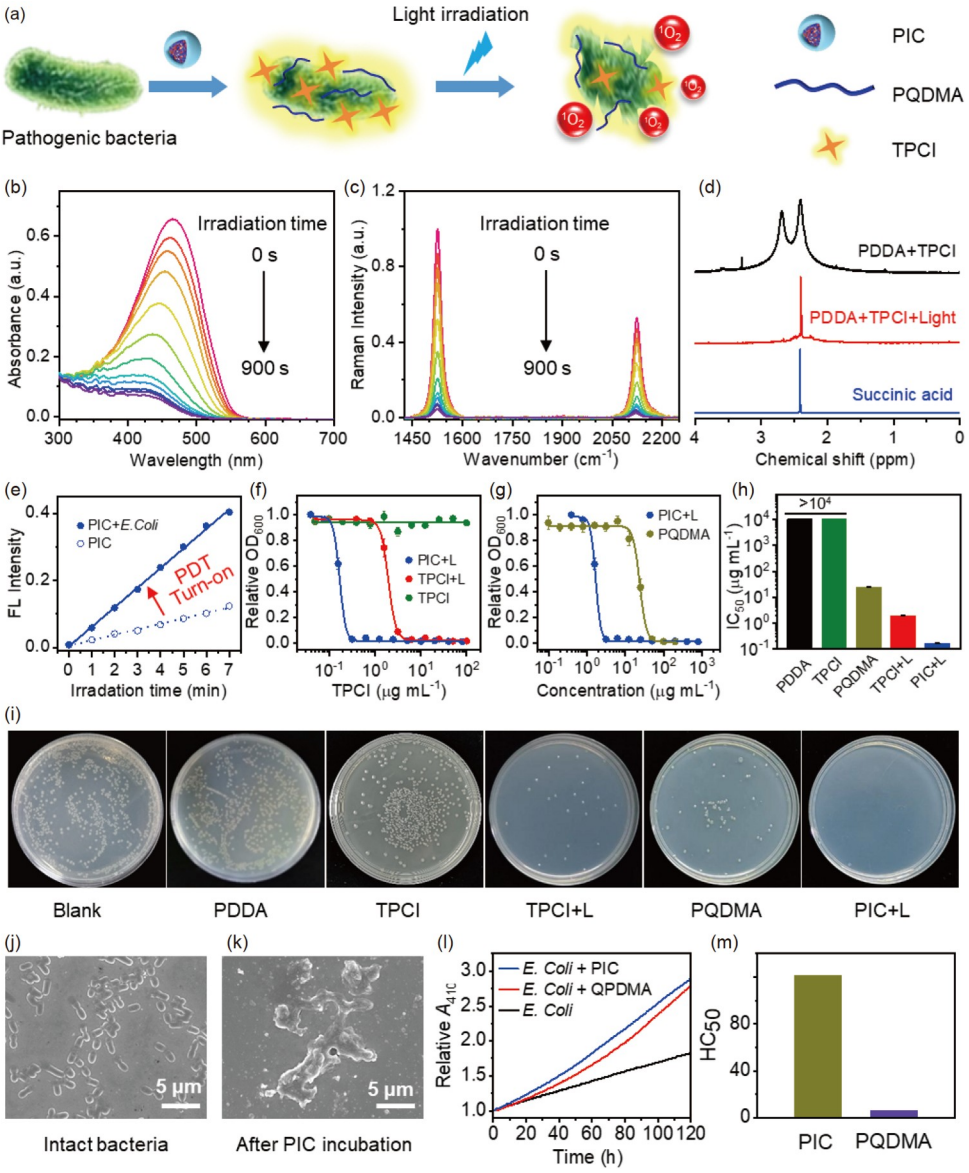

Figure 4 *In vitro* anti-bacterial effect of PIC against *E. coli*. (a) Schematic of the synergistic antibacterial effect of PIC. (b) Absorption spectra of PDDA (25 μg mL^{-1}) in the presence of TPCI (1 μM) upon different irradiation time. (c) Raman spectra of PDDA (25 μg mL^{-1}) in the presence of TPCI (1 μM) upon different irradiation time. (d) ^{1}H NMR spectra of the mixture of PDDA and TPCI without irradiation (PDDA+TPCI), the degradation mixture of PDDA and TPCI after receiving irradiation (PDDA+TPCI+light), and the succinic acid. (e) Fluorescence of DCFDA in the presence of PIC (TPCI: 1 μM) with or without *E. coli* as function of irradiation time. (f) Antibacterial activity of PIC with light irradiation (10 min, PIC+L), TPCI with light irradiation (10 min, TPCI+L), and TPCI without light irradiation (TPCI) as a function of TPCI concentration. (g) Antibacterial activity of PIC with light irradiation (10 min, PIC +L) and PQDMA as a function of PQDMA concentration. (h) Half maximal (50%) bacterial inhibitory concentration of various treatments. (i) Representative images of the *E. coli* culture plates after being treated by PBS, PDDA (25 μg mL^{-1}), TPCI (1 μg mL^{-1}), TPCI (1 μg mL^{-1}) with light irradiation (10 min), PQDMA (10 μg mL^{-1}), and PIC (TPCI: 1 μg mL^{-1}; PQDMA: 10 μg mL^{-1}) with light irradiation (10 min). (j, k) SEM images of *E. coli* before (j) and after (k) being treated with PIC. (l) Membrane permeability experiments of *E. coli* after being treated with PIC or PQDMA. (m) Hemolysis experiment with antibacterial PIC and PQDMA of different concentration. Irradiation in all experiments: λ=450 nm, 5 mW cm^{-2} (color online).

another Gram-negative bacteria *P. aeruginosa* (Figure S9) and a Gram-positive bacteria *S. aureus* (Figure S10). The membrane disruption property of PQDMA is relatively weak on *S. aureus* while the TPCI induced PDT remains destructive. We also used 2-nitrophenyl-β-*D*-galactopyranoside (ONGP) as a probe to evaluate the membrane permeability of the bacteria after being treated with polycations (Figure 4l). The *E. coli* treated with PQDMA or PIC both exhibited an over 2-fold permeability increase than the original *E. coli*, which supported our design to enhance the membrane disruption using polycations. Interestingly, attributed to the strong electrostatic interaction between PQDMA and PDDA, the hemolysis effect of the cationic PQDMA was significantly inhibited in PIC compared with free PQDMA (Figure 4m). These results validated the ROS-deformable PIC as a promising strategy to achieve on-demand release of

cationic antibacterial agents for minimized side effects.

The PIC-enabled fluorescence turn-on detection and PDT turn-on infection inhibition were further verified by CLSM imaging. As shown in Figure 5, the bacteria treated with different conditions were stained with propidium iodide (PI) to display the permeability of the bacteria. For the bacteria treated with free TPCI, only the fluorescence of TPCI was observed, indicating that TPCI alone could not damage the bacteria. On the contrary, the bacteria treated with PQDMA and free TPCI with light both showed strong red PI emission, which proved that they were capable of inducing bacteria damage. As a comparison, when the bacteria were treated with PIC (without light irradiation), the fluorescence of both TPCI and PI could be observed. The relatively weaker fluorescence of the TPCI in the absence of light irradiation clearly demonstrated the fluorescence quenching effect of PDDA. Interestingly, when we further applied light irradiation on the PIC-treated bacteria, the fluorescence of the TPCI was enhanced obviously, mainly because of the ROS-induced deformation of PIC. PI also showed strong fluorescence comparable to the bacteria treated by PQDMA or free TPCI with light, which confirmed that PIC could induce similar membrane disruption effect as PQDMA, and similarly enhanced PDT as free TPCI. These results clearly demonstrated that the PDDA-based PIC is an ideal nanocarrier system for fluorescence and PDT dual turn-on.

2.4 *In vivo* application of antibacterial PIC for infected wound healing

Inspired by the excellent *in vitro* antibacterial theranostic effect of PIC, we further evaluated the *in vivo* antibacterial capacity on wound-infected mouse model. On the back of individual mouse, wound with 1 cm diameter was inflicted and subsequently infected with *P. aeruginosa* (20 μL, 10^8 CFU mL^{-1}). Mice with infected wounds were randomly divided into four groups (n=5 for each group), and each was treated with 20 μL of phosphate buffer saline (PBS) solution, PQDMA solution (10 μg mL^{-1}), TPCI solution (1 μg mL^{-1}), or PIC solution (TPCI: 1 μg mL^{-1}; PQDMA: 10 μg mL^{-1}) on Day 0, 3, 5, and 7, respectively (Figure 6a). For mice treated with TPCI and PIC, 450 nm light irradiation (5 mW cm^{-2}, 20 min) was applied after each drug administration. The wound healing process was investigated for up to 13 days after the treatments started. Representative photographs recording the wound closure during the healing period were compiled in Figure 6b. The wound in the PIC+L group was almost healed on Day 13, whereas those in the other three groups could still be visible. To evaluate the wound healing process quantitatively, the wound area from photographs was calculated (Figure 6c). The PIC+L group showed the fastest wound healing rate, and the wound healing areas for the mice in the PIC+L group were smaller than the mice in other groups on Day 6 and Day 8 (Figure 6d), validating the synergistic antibacterial effect resulted from the PIC. The bacteria from the wound area in each group on Day 3 were collected and counted (Figure 6e). The PIC+L group showed the lowest bacteria colony number, and the PBS group showed the highest. With strong suppressive effect on wound infection by both PDT and membrane disruption, PIC could significantly enhance the survival of infected mice. Compared with the survival rate of 25% in the PBS group, all the mice treated with PIC and irradiation remained alive at the end of the experiment (Figure 6f), indicating the excellent

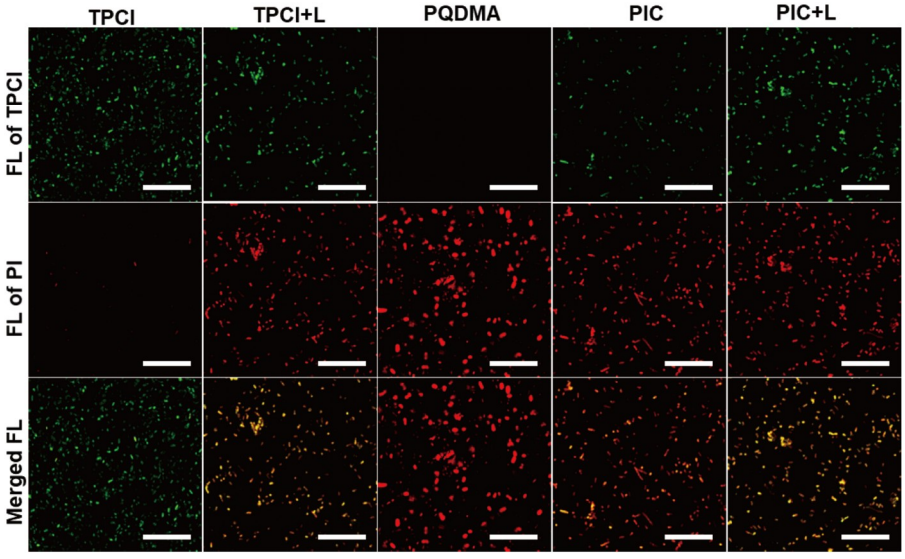

Figure 5 CLSM images of bacteria receiving different antibacterial treatments. All samples were stained with PI. Concentration of TPCI: 1.5 μg mL^{-1}; concentration of PQDMA: 15 μg mL^{-1}; concentrations of TPCI and PQDMA in PIC were 1.5 and 15 μg mL^{-1} respectively. Irradiation: λ=450 nm, 5 mW cm^{-2}, 10 min. TPCI: λ_{ex}=488 nm, fluorescence (FL) was collected from 500 to 550 nm; PI: λ_{ex}=532 nm, FL was collected from 600 to 650 nm. Scale bar: 20 μm (color online).

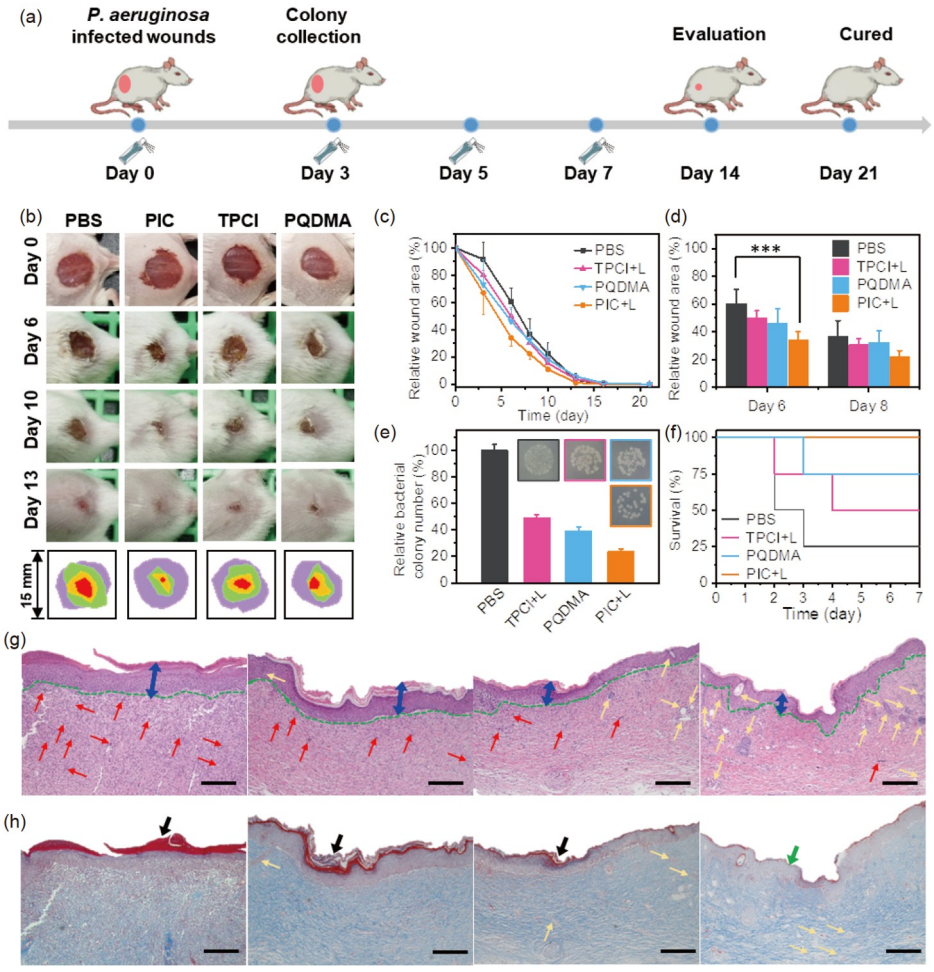

Figure 6 *In vivo* antibacterial effect of mouse wounds infected with *P. aeruginosa*. (a) Schematic diagram of mouse wound infection with *P. aeruginosa* and treatment execution (n=5 for each group). Dosing volume: 20 μL; concentration of PQDMA: 10 μg mL^{-1}; concentration of TPCI: 1 μg mL^{-1}; concentration of PIC: 1 μg mL^{-1} for TPCI and 10 μg mL^{-1} for PQDMA; irradiation: λ=450 nm, 5 mW cm^{-2}, 20 min after administration. (b) Photographs of mouse wounds infected by *P. aeruginosa* receiving different treatments at different time. The last row: representative wound closure traces during the therapy period (the purple, green, yellow, red areas represent the actual wound areas in the corresponding groups on Day 0, 6, 10, 13, respectively). (c) Wound area changes in *P. aeruginosa*-infected mice by time. (d) Relative wound area on Day 6 and Day 8. (e) Colony counting of samples obtained from infected wounds on Day 3. Inset: digital photos of colonies deriving form samples obtained from corresponding infected wounds on Day 3 (the frame colors of photos were consistent with those in the bar chart). (f) Survival rates of *P. aeruginosa*-infected mice receiving different treatments. (g) H&E staining and (h) masson staining of infected skin wound tissue with different treatments on Day 14. Green dashed lines: the boundary of epithelium and dermis; blue double-headed arrows: granulation tissues; red arrows: inflammatory cells; yellow arrows: hair follicles; black arrows: damaged epidermis; green arrows: complete epidermis. Scale bar: 200 μm (color online).

alleviation of bacterial infection as well as the fast wound healing by the synergistic membrane disruption and turned-on PDT through PIC.

To further assess the wound repair process, the wounds of mice were harvested and subjected to hematoxylin and eosin (H&E) staining and Masson's trichome staining on Day 14. As shown in Figure 6g, the granulation tissues (blue double-head arrows) in the PBS group were thicker than those in all other groups, whereas those in the PIC+L group was the thinnest, suggesting a better regeneration of epithelial tissues in the PIC+L group. The epidermis in the PBS group was severely damaged, and incomplete epidermis could also be observed in TPCI and PQDMA group (Figure 6h, black arrows). In contrast, infected tissues in the PIC+L group formed completely regenerated epithelium (Figure 6h, green arrow). Additionally, hair follicles (marked by the yellow arrows), one of the dermal appendages for the structural integrity of the remodeling tissue evaluation were also more intensive in the PIC+L group, illustrating that the dermis was reforming and PIC achieved the best wound healing effects among all therapies. Moreover, less inflammatory cells (marked by the red arrows) indicated that wounds in the PIC+L group had already undergone the inflammatory phase and were in a later wound healing stage. These data confirmed that the synergistic bacterial elimination ability offered by PIC can effectively promote the infected wound healing process, validating PIC as an excellent wound dressing material with great clinical application potentials.

3 Conclusions

In summary, we have created an antibacterial PIC based on anionic polydiacetylene PDDA to realize the AIE turn-on detection and on-demand eradication of pathogen bacteria. With the excellent absorption effect of PDDA, the AIE of TPCI is efficiently quenched in the PIC, so that the turn-on detection of bacteria by TPCI can be achieved conveniently and sensitively. It is also noteworthy that the ROS generation efficiency of TPCI in PIC fluorescence can also be turned-on in the presence of bacteria. Upon the on-demand light irradiation, the PIC is deformed by the generated ROS to completely release TPCI and PQDMA for synergistic PDT and membrane disruption on the bacteria. The efficient antibacterial activities against both Gram-negative and Gram-positive bacteria were validated at low concentrations, and the antibacterial PIC also accelerated the wound closure of *P. aeruginosa*-infected mice. This polydiacetylene-based PIC system not only holds great promise in fighting against pathogen bacteria, but also sheds new light for the development of "turn-on" fluorescence sensing and imaging systems based on AIE lumigens.

Acknowledgements This work was supported by the National Natural Science Foundation of China (21877042, 22077038, 22107032), the National Basic Research Plan of China (2018YFA0208903), Postdoctoral Research Foundation of China (2017M622454, 2020T130038ZX), and Huazhong University Startup Fund.

Conflict of interest The authors declare no conflict of interest.

Supporting information The supporting information is available online at http://chem.scichina.com and http://link.springer.com/journal/11426. The supporting materials are published as submitted, without typesetting or editing. The responsibility for scientific accuracy and content remains entirely with the authors.

1 Lewis K. *Nat Rev Drug Discov*, 2013, 12: 371–387
2 Aminov RI. *Front Microbiol*, 2010, 1: 134
3 Gaynes R. *Emerg Infect Dis*, 2017, 23: 849–853
4 Bush K, Courvalin P, Dantas G, Davies J, Eisenstein B, Huovinen P, Jacoby GA, Kishony R, Kreiswirth BN, Kutter E, Lerner SA, Levy S, Lewis K, Lomovskaya O, Miller JH, Mobashery S, Piddock LJV, Projan S, Thomas CM, Tomasz A, Tulkens PM, Walsh TR, Watson JD, Witkowski J, Witte W, Wright G, Yeh P, Zgurskaya HI. *Nat Rev Microbiol*, 2011, 9: 894–896
5 Blair JMA, Webber MA, Baylay AJ, Ogbolu DO, Piddock LJV. *Nat Rev Microbiol*, 2015, 13: 42–51
6 Neu HC. *Science*, 1992, 257: 1064–1073
7 Nathan C, Cars O. *N Engl J Med*, 2014, 371: 1761–1763
8 Cattoir V, Felden B. *J Infect Dis*, 2019, 220: 350–360
9 Wang Y, Yang Y, Shi Y, Song H, Yu C. *Adv Mater*, 2020, 32: 1904106
10 Livermore DM. *Lancet Infect Dis*, 2005, 5: 450–459
11 Chernousova S, Epple M. *Angew Chem Int Ed*, 2013, 52: 1636–1653
12 Qi L, Xu Z, Jiang X, Hu C, Zou X. *Carbohydr Res*, 2004, 339: 2693–2700
13 Sudarshan NR, Hoover DG, Knorr D. *Food Biotechnol*, 1992, 6: 257–272
14 Hilpert K, Volkmer-Engert R, Walter T, Hancock REW. *Nat Biotechnol*, 2005, 23: 1008–1012
15 Boman HG. *J Intern Med*, 2003, 254: 197–215
16 Deka SR, Sharma AK, Kumar P. *Curr Trends Med Chem*, 2015, 15: 1179–1195
17 Guo J, Qin J, Ren Y, Wang B, Cui H, Ding Y, Mao H, Yan F. *Polym Chem*, 2018, 9: 4611–4616
18 Xu JW, Yao K, Xu ZK. *Nanoscale*, 2019, 11: 8680–8691
19 Chen Y, Gao Y, Chen Y, Liu L, Mo A, Peng Q. *J Control Release*, 2020, 328: 251–262
20 Liu Y, Qin R, Zaat SAJ, Breukink E, Heger M. *J Clin Transl Res*, 2015, 1: 140–167
21 Cao S, Shao J, Abdelmohsen LKEA, Hest JCM. *Aggregate*, 2022, 3: e128
22 Ding X, Duan S, Ding X, Liu R, Xu FJ. *Adv Funct Mater*, 2018, 28: 1802140
23 Cloutier M, Mantovani D, Rosei F. *Trends Biotechnol*, 2015, 33: 637–652
24 Mura S, Nicolas J, Couvreur P. *Nat Mater*, 2013, 12: 991–1003
25 Zheng P, Liu Y, Chen J, Xu W, Li G, Ding J. *Chin Chem Lett*, 2020, 31: 1178–1182
26 Janib SM, Moses AS, MacKay JA. *Adv Drug Deliver Rev*, 2010, 62: 1052–1063
27 Xie J, Lee S, Chen X. *Adv Drug Deliver Rev*, 2010, 62: 1064–1079
28 Lammers T, Aime S, Hennink WE, Storm G, Kiessling F. *Acc Chem Res*, 2011, 44: 1029–1038
29 Wang L, Li LL, Ma HL, Wang H. *Chin Chem Lett*, 2013, 24: 351–358
30 Traba C, Liang JF. *J Control Release*, 2015, 198: 18–25
31 Wei T, Yu Q, Chen H. *Adv Healthcare Mater*, 2019, 8: 1801381
32 Moorcroft SCT, Jayne DG, Evans SD, Ong ZY. *Macromol Biosci*, 2018, 18: 1800207
33 Li Q, Zhang Y, Huang X, Yang D, Weng L, Ou C, Song X, Dong X. *Chem Eng J*, 2021, 407: 127200
34 Canaparo R, Foglietta F, Giuntini F, Della Pepa C, Dosio F, Serpe L. *Molecules*, 2019, 24: 1991
35 Pang Q, Zheng X, Luo Y, Ma L, Gao C. *J Mater Chem B*, 2017, 5: 8975–8982
36 Amstad E, Kim SH, Weitz DA. *Angew Chem Int Ed*, 2012, 51: 12499–12503
37 Pitt WG, Husseini GA, Staples BJ. *Expert Opin Drug Deliver*, 2004, 1: 37–56
38 Geilich BM, Gelfat I, Sridhar S, van de Ven AL, Webster TJ. *Biomaterials*, 2017, 119: 78–85
39 Parisi OI, Scrivano L, Sinicropi MS, Puoci F. *Curr Opin Pharmacol*, 2017, 36: 72–77
40 Leung NLC, Xie N, Yuan W, Liu Y, Wu Q, Peng Q, Miao Q, Lam JWY, Tang BZ. *Chem Eur J*, 2014, 20: 15349–15353
41 Zeng Q, Li Z, Dong Y, Di C, Qin A, Hong Y, Ji L, Zhu Z, Jim CKW, Yu G, Li Q, Li Z, Liu Y, Qin J, Tang BZ. *Chem Commun*, 2007, 1: 70–72
42 Kang M, Zhang Z, Song N, Li M, Sun P, Chen X, Wang D, Tang BZ. *Aggregate*, 2020, 1: 80–106
43 Lou X, Yang Y. *Aggregate*, 2020, 1: 19–30
44 Tian S, Yue Q, Liu C, Li M, Yin M, Gao Y, Meng F, Tang BZ, Luo L. *J Am Chem Soc*, 2021, 143: 10054–10058
45 Li Y, Hu X, Tian S, Li Y, Zhang G, Zhang G, Liu S. *Biomaterials*, 2014, 35: 1618–1626
46 Tian S, Liu G, Wang X, Wu T, Yang J, Ye X, Zhang G, Hu J, Liu S. *ACS Appl Mater Interfaces*, 2016, 8: 3693–3702
47 Tian S, Li H, Li Z, Tang H, Yin M, Chen Y, Wang S, Gao Y, Yang X, Meng F, Lauher JW, Wang P, Luo L. *Nat Commun*, 2020, 11: 81
48 Gao Y, Wang X, He X, He Z, Yang X, Tian S, Meng F, Ding D, Luo L, Tang BZ. *Adv Funct Mater*, 2019, 29: 1902673